Chapter 6

Robust Controller Design

Renewable energy based microgrid systems are vital to the fulfilment of present day energy needs of the market. The majorly available inexhaustible sources: solar energy and fuel cells are DC-based whereas, wind energy is AC in nature. The focus of the preceding three chapters is on microgrid stability and modelling, determining the small signal model and its reduced order equivalent of the complex AC and DC microgrid system in terms of state space representations. Power transfer in AC and DC microgrid systems is in the form of AC currents and voltages and DC currents and voltages, respectively. In an AC microgrid system, the AC loads require single conversion stage whereas DC loads require multiple conversion stages. Similarly, DC microgrid contains single conversion for DC loads and multiple conversion stages for AC loads. Thus, the combination of the AC and the DC microgrid is termed as Hybrid Microgrid systems, which facilitates the connectivity of the AC and DC loads and sources to the power system to minimize the conversion losses [95-96]. This results in the emergence of the critical issue of proper integration of various naturally available AC-DC sources to the AC-DC loads and the main utility grid. Efficient energy and load sharing is also a key factor in such hybrid systems. The AC to DC conversion from AC microgrid section to DC microgrid section and vice-versa, is achieved by intermediate Interlinking Converters (ICs) which are generally bidirectional in nature. A block diagram of the hybrid microgrid with separate DC and AC sections and interfacing ICs is depicted in Figure 6.1.

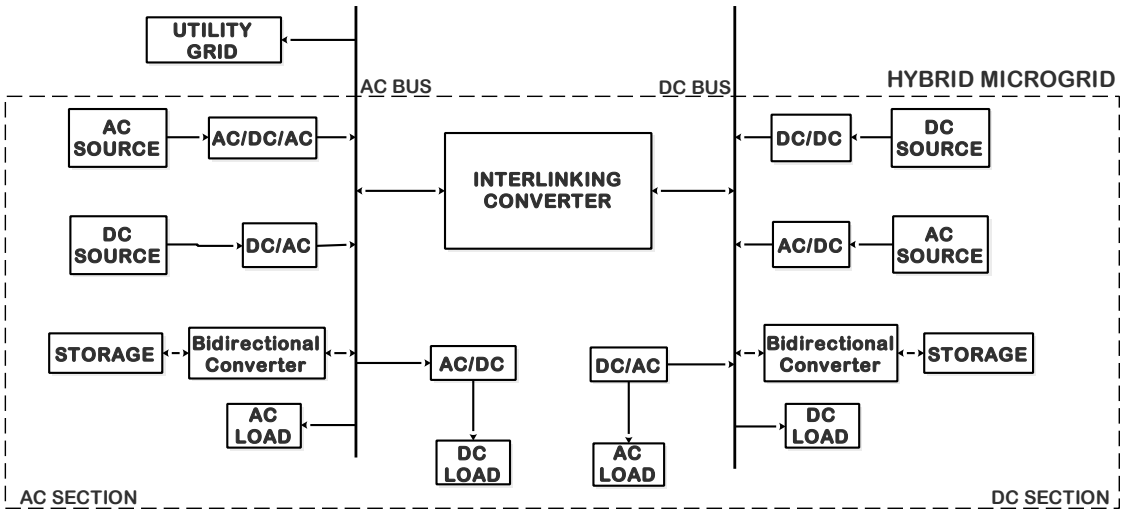

Figure 6.1. *Block diagram of Hybrid Microgrid.*

The figure consists of AC and DC source and loads with their appropriate interfacing power electronics devices connected as two separable bus sections through an IC block. ICs are basically power electronic circuits which act as an interface between AC and DC sections of a hybrid microgrid with the main functions of effective energy sharing and maintaining the constant DC voltage across DC load. A simplified AC to DC interlinking converter whose circuit diagram is shown in Figure 6.2 has been considered in this work for optimal controller design. The converter structure consists of a three-phase AC source connected to a six-switch IGBT/diode rectifier bridge via RL filter connected on the three input phases. The rectified output is connected to a resistive DC load through a DC link capacitor to smooth out the ripples in the DC output.

The small signal modelling of this converter system in the subsequent section aids in subsequent controller design and analysing the stability of the controlled converter model. This chapter presents robust controller design via adaptive parameter tuning through swarm intelligence techniques. It consists of design of PID, FOPID and H_∞ loop

shaping controllers through ABC and PSO tuning algorithms and comparison of their simulation results in the form of a case study.

6.1 Preliminaries

Some of the preliminary concepts to robust controller design for interlinking converter are given in this section.

6.1.1 Robustness and Performance

Robustness is the ability of the closed loop system to be immune to uncertainties in the system components. It is the key factor in the design of feedback systems and hence needs to be discussed prior to the closed loop analysis of the control system. Moreover, performance and robustness are two closely related properties. Where disturbance and robustness are determined by feedback, the performance is mostly related to the feed-forward action of tracking the reference signal. These can be measured quantitatively by a group of six transfer functions, termed as 'Gang of Six'.

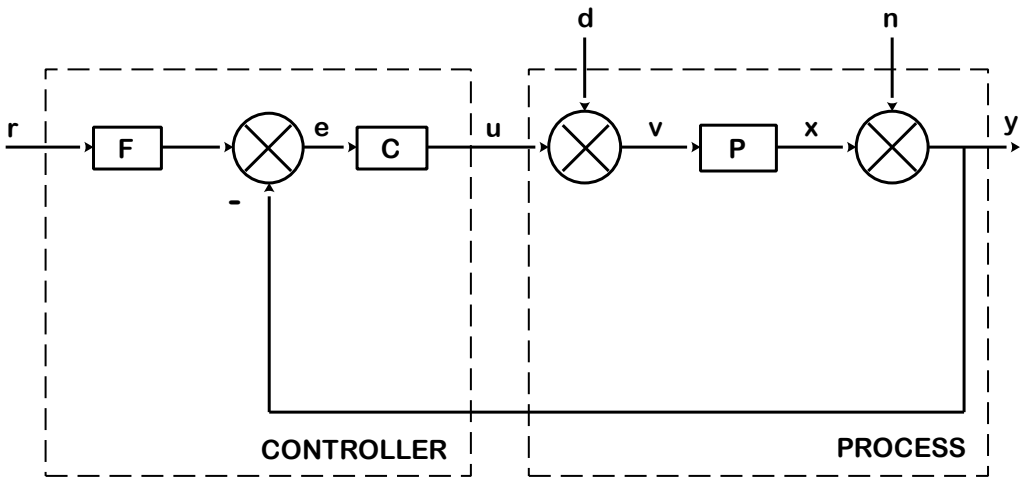

Figure 6.2. *Basic feedback configuration.*

Figure 6.2 shows a feedback control configuration where, three external inputs, reference signal, r, load disturbance, d and measurement noise n affect the feedback law. The set of all six transfer functions of the system as in [97-98] are;

$$\frac{\boldsymbol{PCF}}{\boldsymbol{1+PC}} \qquad \frac{\boldsymbol{PC}}{\boldsymbol{1+PC}} \qquad \frac{\boldsymbol{P}}{\boldsymbol{1+PC}}$$

$$\frac{\boldsymbol{CF}}{\boldsymbol{1+PC}} \qquad \frac{\boldsymbol{C}}{\boldsymbol{1+PC}} \qquad \frac{\boldsymbol{1}}{\boldsymbol{1+PC}} \tag{6.1}$$

When $F = 1$, the system is in pure error feedback configuration and is characterised by four of the above six transfer functions as;

$\frac{PC}{1+PC}$: Complementary sensitivity function

$\frac{P}{1+PC}$: Load disturbance sensitivity function (Input sensitivity function)

$\frac{C}{1+PC}$: Noise sensitivity function (Output sensitivity function)

$\frac{1}{1+PC}$: Sensitivity function

Thus, this '*Gang of Four'* transfer functions[97] give an insight into the system robustness and performance with changes in the operating conditions and system components. These parameters play a vital role in the controller design of the hybrid microgrid system under consideration and are thus discussed here in this subsection.

6.1.2 Linear Quadratic Regulator design

Linear Quadratic Regulator (LQR) is the optimal theory of pole placement method. LQR algorithm defines the optimal pole location based on two cost function. Before designing the LQR controller for a linear state space model, certain characteristics of

model like stability, controllability and observability, are to be analysed for adequate system performance [99-100].

LQR is an optimal controller, based on state feedback method. With all controllable states, it minimizes the performance index of a linear system given as [101-102];

$$\dot{x} = Ax + Bu \tag{6.2}$$

For the linearized system given in equation (6.2), with infinite final time, the quadratic Performance Index (PI) is given as:

$$J = \frac{1}{2}\int_0^\infty [x^T(t)Q(t)x(t) + u^T(t)R(t)u(t)]dt \tag{6.3}$$

The PI is to be minimized by the control input,u given as,

$$u = -kx \tag{6.4}$$

where,

$$k = R^{-1}B^T P \tag{6.5}$$

and Q and R are positive semi definite and positive definite weighing matrices respectively.

Q and R, given in equation (6.3), are error weight matrices which constitute the relative effect of states and control inputs respectively to the final objective function of the given system. For efficient LQR controller design, these matrices are to be selected to effectively minimize the performance index (PI) given in as *J*.

The matrices Q and R are chosen to be diagonal so that the objective function *J* is kept squared positive, given as;

$$J = q_1 x_1^2 + q_2 x_2^2 + \cdots + r_1 u^2 \tag{6.6}$$

The LQR technique gives effective system performance and is used in designing a controller for the higher and lower order control system to achieve required performance specifications.

6.1.3 Small Signal Modelling of Interlinking Converter

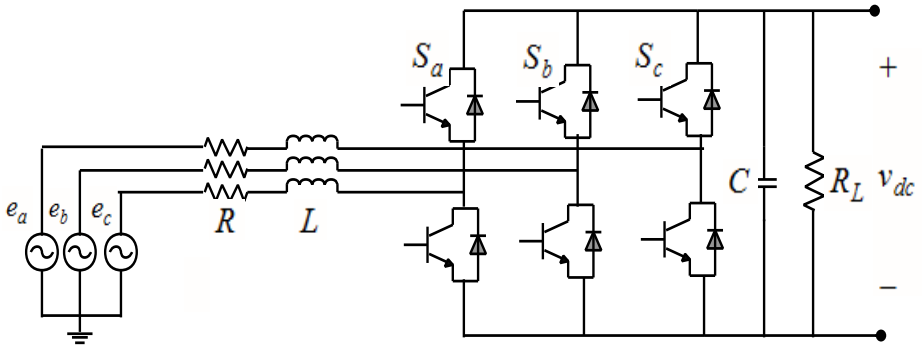

Figure 6.3. *Circuit diagram of Interlinking Converter.*

The schematic diagram of IC in Figure 6.3 consists of a three phase ac source, RL filter, three phase six-switch bridge rectifier, dc link capacitor and a dc load (resistive). The main aim of this paper is to control the filter current and dc link voltage through proper switching pulses at the bridge switches.

The differential equations for the mathematical modelling of the interlinking converter for AC to DC conversion operation[65], considering the basic concept of current through input inductors and the voltage across output capacitor as state variables in d-q frames are written as;

$$\dot{i_d} = -\frac{R}{L}i_d + \frac{1}{L}e_d + \omega i_q - \frac{S_d}{L}v_{dc} \tag{6.7}$$

$$\dot{i_q} = -\frac{R}{L}i_q + \frac{1}{L}e_q - \omega i_d - \frac{S_q}{L}v_{dc} \tag{6.8}$$

$$\dot{v_{dc}} = \frac{3}{2C}(S_q i_q + S_d i_d) - \frac{1}{CR_L} v_{dc} \tag{6.9}$$

where, i_{dq} are the current flowing through the inductor on ac side in d-q axis; e_{dq} are the ac source voltages in d-q axis; S_{dq} are the switching sequence functions in d-q axis; v_{dc} is the dc voltage at output across the load; R_L is the load resistance; ω is the operating frequency of the system; R and L are the input filter parameters and C is the dc link capacitor.

$$x_1 = i_d; x_2 = i_q;\ x_3 = v_{dc} \tag{6.10}$$

$$u_1 = S_d;\ u_2 = S_q; u_3 = v_d \tag{6.11}$$

After the substitutions for inputs and state variables as in (6.10-6.11) into mathematical equations in (6.7-6.9), the MIMO non-linear state-space model of the converter is given as in (6.12).

$$\dot{x} = \begin{bmatrix} -\frac{R}{L}x_1 + \omega x_2 \\ -\frac{R}{L}x_2 - \omega x_1 \\ -\frac{x_3}{CR_L} \end{bmatrix} + \begin{bmatrix} -\frac{x_3}{L} & 0 & \frac{1}{L} \\ 0 & -\frac{x_3}{L} & 0 \\ \frac{3x_1}{2C} & \frac{3x_2}{2C} & 0 \end{bmatrix} u \tag{6.12}$$

The small-signal interlinking converter model obtained through the linearization of the nonlinear state space (6.12) around a stable operating point, evaluated by equating it to zero and considering small state perturbations is rewritten in the standard form as (6.13).

$$\dot{x} = Ax + Bu; y = Cx \tag{6.13}$$

where the jacobian matrices are obtained as;

$$A = \begin{bmatrix} -\frac{R}{L} & \omega & -\frac{U_1}{L} \\ -\omega & -\frac{R}{L} & -\frac{U_2}{L} \\ \frac{3U_1}{2C} & \frac{3U_2}{2C} & -\frac{1}{R_L C} \end{bmatrix};\ B = \begin{bmatrix} -\frac{X_3}{L} & 0 & \frac{1}{L} \\ 0 & -\frac{X_3}{L} & 0 \\ \frac{3X_1}{2C} & \frac{3X_2}{2C} & 0 \end{bmatrix};\ C = \begin{bmatrix} 1 & 0 & 0 \\ 0 & 1 & 0 \\ 0 & 0 & 1 \end{bmatrix} \tag{6.14}$$

Thus, the state space model of the interlinking converter consists of three states and is utilised for the controller design formulation discussed in the next sections.

6.2 Robust control of Interlinking Converter model

In this thesis, the robust controller design of interlinking converter model has been achieved through adaptive tuning of controller parameters so as to enhance robustness to noise and system uncertainties. Three controllers have been considered in this analysis, namely; PID, FOPID and H_∞ loop shaping controller, for tuning through PSO and ABC optimization algorithms.

6.2.1 PID and FOPID controller

Proportional-Integral-Derivative (PID) control is the feedback control mechanism which combines the proportional, derivative and integral actions to control the process variable and automatically adjust it as close as possible to the set-point or reference. A block diagram for feedback control is given in Figure 6.4. The PID controller transfer function is given in (6.15). This is the simplest type of controller and gives accurate analysis over a wide range of applications. However, the controller response varies with parameter changes, and its performance degrades over time. This may even lead to instability or errors in the output. Only three unknown controller specifications (k_P, k_I, k_D) are to be tuned which also limits the tuning strategy.

$$K_{PID}(s) = k_P + \frac{k_I}{s} + k_D s \tag{6.15}$$

Fractional Order Proportional-Integral-Derivative (FOPID) controller is an enhancement over the traditional PID control based on fractional calculus. It is characterized by five parameters, i.e. the Proportional gain (k_P) the integral gain (k_I), the

derivative gain (k_D), integral order (λ) and derivative order (μ), thereby increasing the opportunity for tuning strategies involved in achieving better control. This type of control is highly immune to parameter variations and thus more robust [103]. Further, most of the practical systems are fractional order systems described by fractional order integro-differential equations rather that integer order. Therefore, FOPID controller design for these systems is particularly more significant. Its transfer function is represented as in (6.16).

$$K_{FOPID}(s) = k_P + \frac{k_I}{s^{\lambda}} + k_D s^{\mu} \tag{6.16}$$

In the controller design problem, optimization techniques are increasingly being used for automatic and self-adaptive tuning of the various controller parameters. Efficient tuning of these parameters such as $k_P, k_I, k_D, \lambda, \mu$ in FOPID control scheme can achieve desired control objectives for various operating conditions. The swarm based optimization algorithms have gained popularity in various control related formulations due to their social interactive and self-organising problem-solving mechanisms. Two of the most popular swarm intelligence algorithms; PSO and ABC have been considered for optimal parameter tuning in this analysis and are discussed in detail in Section 4.1 in Chapter 4.

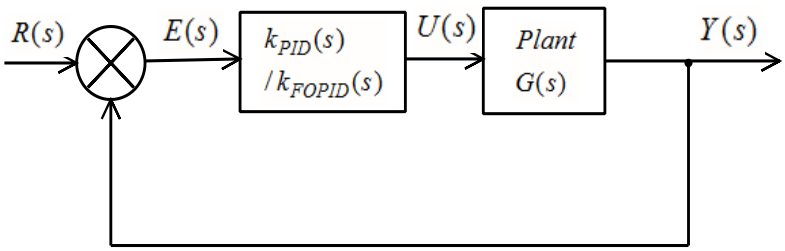

Figure 6.4. *Block diagram of the closed-loop system with PID/FOPID controller.*

6.2.2 Loop shaping controller design

This section is further divided into three parts: *Augmented Plant Model* derives a mathematical model of the standard augmented plant *P*, as shown in Figure 6.5 which is directly used in controller design. *H-Infinity Loop Shaping Feedback Controller Design Formulation* gives the various definitions and inequalities of H-infinity loop shaping controller, the constraints on the weight functions with reference to the sensitivity and complementary sensitivity functions. *Optimization of Weight Functions* determines a method for obtaining the optimized weight functions through ABC algorithm such that both performance and robustness can be attained.

6.2.2.1 Augmented Plant Model

A closed-loop plant *P* formed by the converter model, weighting functions and controller is shown in Figure 6.5 is mathematically expressed as;

$$\begin{bmatrix} z \\ y \end{bmatrix} = \boldsymbol{P} \begin{bmatrix} w \\ u \end{bmatrix} \tag{6.17}$$

where u and w are the control and exogenous (reference) inputs respectively; y and z are the measured and controlled outputs.

Considering the state-space model of the plant of the form;

$$\dot{x_g} = A_g x_g + B_g u;\ y_g = C_g x_g \tag{6.18}$$

where, x_g is the plant state vector and $(A_g, B_g, C_g, 0)$ is the state-space representation of the plant model.

The state space realizations for the two weighing functions are given as;

$$\dot{x_{w1}} = A_{w1} x_{w1} + B_{w1}(w - y_g) = -B_{w1} C_g x_g + A_{w1} x_{w1} + B_{w1} w;$$

$$z_1 = C_{w1} x_{w1} + D_{w1}(w - y_g) \tag{6.19}$$

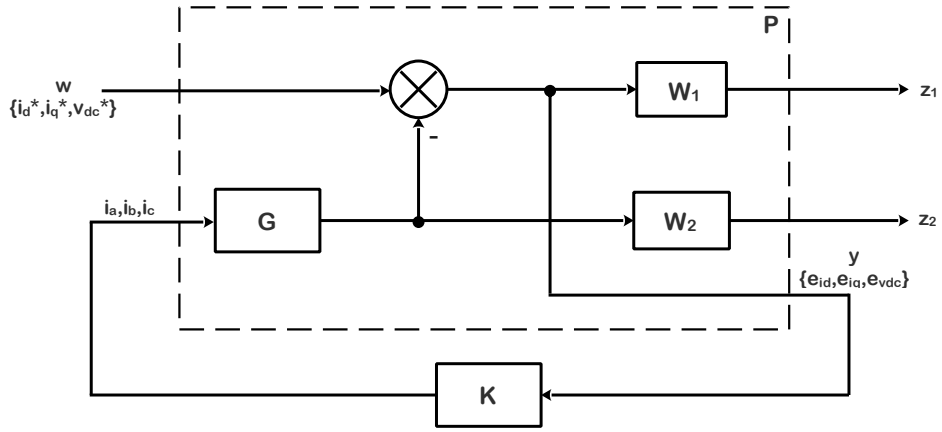

Figure 6.5. *H-infinity loop shaping controller design formulation.*

$$\dot{x_{w2}} = A_{w2}x_{w2} + B_{w2}y_g = B_{w2}C_g x_g + A_{w2}x_{w2};\ z_2 = C_{w2}x_{w2} + D_{w1}y_g \tag{6.20}$$

where, x_{w1} and x_{w2} are the two weight function state vectors; $(A_{w1}, B_{w1}, C_{w1}, 0)$ and $(A_{w2}, B_{w2}, C_{w2}, 0)$ are their state-space representations.

Thus the linearized state-space model of the overall plant is evaluated and rearranged in the standard form in equation (6.21).

$$\dot{x} = Ax + B_1 w + B_2 u$$

$$z = C_1 x + D_{11} w + D_{12} u$$

$$y = C_2 x + D_{21} w + D_{22} u \tag{6.21}$$

where; $x = [x_g \quad x_{w1} \quad x_{w2}]^T;\ z = [z_1 \quad z_2]^T$

Thus, the representation of the augmented plant [101-102] is,

$$P(s) := \begin{bmatrix} P_{11} & P_{12} \\ P_{21} & P_{22} \end{bmatrix} = \begin{bmatrix} D_{11} & D_{12} \\ D_{21} & D_{22} \end{bmatrix} + \begin{bmatrix} C_1 \\ C_2 \end{bmatrix} (sI - A)^{-1} [B_1 \quad B_2] = \begin{bmatrix} A & B_1 & B_2 \\ C_1 & D_{11} & D_{12} \\ C_2 & D_{21} & D_{22} \end{bmatrix} \tag{6.22}$$

where, the state space matrices are evaluated to be;

$$A = \begin{bmatrix} A_g & 0 & 0 \\ -B_{w1}C_g & A_{w1} & 0 \\ B_{w2}C_g & 0 & A_{w2} \end{bmatrix}; B_1 = \begin{bmatrix} 0 \\ B_{w1} \\ 0 \end{bmatrix}; B_2 = \begin{bmatrix} B_g \\ 0 \\ 0 \end{bmatrix}; C_1 = \begin{bmatrix} -C_g D_{w1} & C_{w1} & 0 \\ C_g D_{w2} & 0 & C_{w2} \end{bmatrix};$$

$$D_{11} = \begin{bmatrix} D_{w1} \\ 0 \end{bmatrix}; D_{12} = \begin{bmatrix} 0 \\ 0 \end{bmatrix}; C_2 = [-C_g \quad 0 \quad 0]; D_{21} = 1; D_{22} = 0 \tag{6.23}$$

For the interlinking converter system under consideration, the control input $u = [S_d\ S_q\ v_d]$; the reference input $w = \left[i_d^*\ i_q^*\ v_{dc}^*\right]$ and the measured or error output $y = [e_{id}\ e_{iq}\ e_{vdc}]$. As discussed in Section 6.1, x_g is a three state vector of the converter model. x_{w1} and x_{w2} are of three state each corresponding to the three plant output and error output variables.

6.2.2.2 H-Infinity Loop Shaping Feedback Controller Design Formulation

For a controller $K(s)$ connecting the plant output y to plant input u, the requirement of H_∞ loop shaping controller design problem is the formulation of a controller $K(s)$ which makes the closed loop system internally stable and minimizes its H_∞ norm.

The closed-loop system in Figure 6.5, can be expressed as;

$$z = [P_{11} + P_{12}K(I - P_{22}K)^{-1}P_{21}]w = F_l(P,K)w \tag{6.24}$$

Minimization of $\|F_l(P,K)\|_\infty$ is equivalent to minimization of γ such that

$$\|F_l(P,K)\|_\infty < \gamma \Rightarrow \left\| \begin{matrix} W_1 S \\ W_2 T \end{matrix} \right\|_\infty < \gamma \tag{6.25}$$

Thus, the objective of the H_∞ loop shaping controller is to shape the sensitivity and complementary sensitivity functions, S and T respectively, by properly tuning their weights W_1 and W_2 such that the lower fractional transformation (L.F.T.) function, $F_l(P,K)$ is minimised [73,106-107]. It also aims to achieve a stable closed loop system. The two weight functions are to be properly chosen so that the loop shaping control

achieves the desired objective of enhanced system performance. These functions are selected such that; W_1 is to be chosen such that the gain within the desired control bandwidth is high for increased disturbance rejection, i.e., reduced tracking error; W_2 is to be chosen such that the gain outside the control bandwidth is high for good stability margins, i.e., increased robustness. Thus, a trade-off between reduced tracking error and robustness is to be achieved by proper selection of weighing functions.

6.2.2.3 Optimization of Weight Functions

Proper selection of the weight functions W_1 and W_2 requires the fulfilment of three loop shaping conditions. The first two conditions are determined from the constraint of LFT minimization as in the previous subsection such that;

$$\|W_1 S\|_\infty < 1 \tag{6.26}$$

$$\|W_2 T\|_\infty < 1 \tag{6.27}$$

The third condition requires the 0-dB crossover frequency of W_1 to be sufficiently below 0-dB crossover frequency of $1/W_2$ which can also be confirmed in our controller design by fulfilling the relationship [73];

$$S + T = 1 \tag{6.28}$$

Considering the general form of the weights as in (6.29-6.30), the selection criterion is based on the determination of certain parameters involved so that the loop shaping controller achieves the required performance measure.

$$W_1 = a\frac{s/g+\omega_{BW}}{s+h\omega_{BW}} \tag{6.29}$$

$$W_2 = b\frac{s+\omega_{BW}/g}{hs+\omega_{BW}} \tag{6.30}$$

where, a, b are the scaling factors for W_1 and W_2 respectively; g is the peak amplitude; h is the maximum allowed offset at steady state and ω_{BW} is the desired system bandwidth.

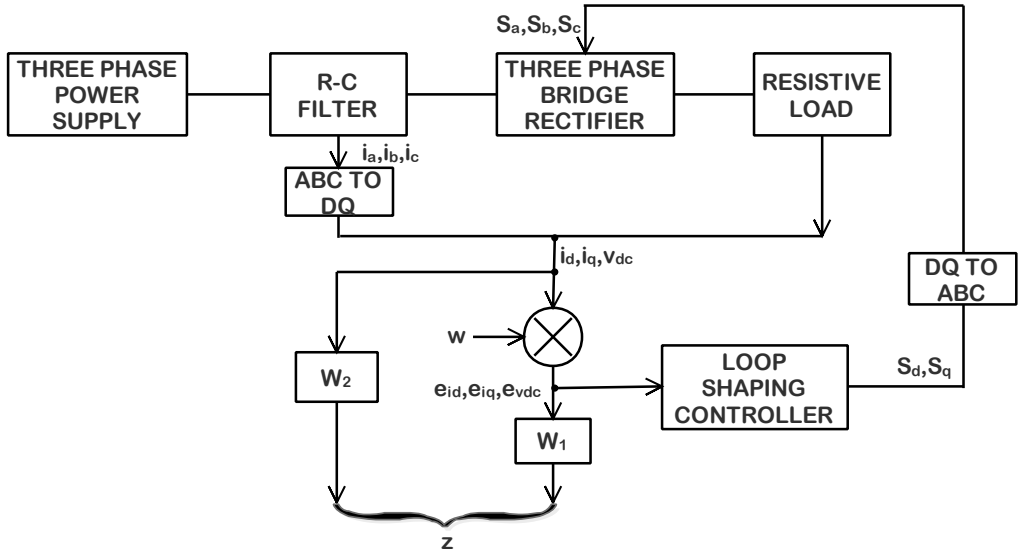

Figure 6.6*. H-infinity loop shaping controller configuration for IC.*

By fixing the value of maximum offset to 0.0001, the optimum values of remaining 4 variables is to be obtained so as to fulfil the above discussed conditions. In general controller design problems these parameters are determined by trial and error method. For better weight selection process, these variables can be optimized through various optimization tools available. ABC being the most versatile and effective optimization algorithm has been utilised for the evaluation of these weight functions.

It is worthy to mention that, the efficacy of the H-infinity loop shaping controller design is embedded in the inherit quality of reducing the tracking errors, increasing the system robustness and achieving the bandwidth requirements. The automatic noise attenuation, system perturbations and unknown uncertainties make this controller suitable for application to mathematical models of systems prone to unpredictable system changes, for example, the interlinking converter for hybrid based systems. Therefore, in

this work, the control strategy is designed for an augmented configuration of the converter state space model incorporating properly selected weight functions. A proper selection of these weights ensures adequate system performance in tracking errors and uncertainties. It incorporates a weight selection mechanism based on optimization of the weight parameters according to the PSO and ABC optimization algorithms. These algorithms provide nature inspired mathematical tool for evaluating optimal parameter values with optimal performance index within certain constraints. Thus, the optimized weights achieve better controller performance due to the adaptive and versatile swarm intelligence algorithm.

6.3 Simulation Results

The simulation results obtained for the robust control of interlinking converter in MATLAB 2016a have been given in this section. Tuning of controller parameters is performed in MATLAB environment and the optimization coding is simulated with Intel(R) Core™ i5-5200U CPU 2.20GHz (4.00 GB RAM).

6.3.1 Controller design through PSO and ABC algorithm

The state space model of the IC system as in equation (6.13) has been developed with the circuit parameters as given in Table 6.1. for subsequent controller design for proper control of the switching of the inverter system. Proper tuning of the controller parameters, i.e., (k_P, k_I, k_D) in PID, $(k_P, k_I, k_D, \lambda, \mu)$ in FOPID controller and $(a, b, g, \omega_{BW}, h)$ in loop shaping controller, is essential to achieve the required closed loop system behaviour of high robustness and immunity to variations. These parameters can automatically be tuned through optimization techniques by simple programming procedures.

Table 6.1. IC circuit parameter values.

S.No.	Parameter	Value	S.No.	Parameter	Value
1	*Rated Power*	1kVA	**5**	R	4 Ω
2	*Grid voltage*	400 V	**6**	L	165 mH
3	*Grid Frequency*	60 Hz	**7**	C	2 mF
4	*Switching frequency*	3000 Hz	**8**	R_L	100 Ω
			9	e_d	380 V

PSO and ABC optimization algorithms have been used for optimal parameter tuning of the three control strategies in this analysis, such that the objective function or fitness function in all of the cases is same for generality and is defined as the H-infinity norm of the closed loop feedback system of the IC with the controller, i.e.,

$$J(G,K) = \|feedback(G,K)\|_\infty \tag{6.31}$$

i.e., **Minimize** $\left\|\frac{\boldsymbol{G}}{\boldsymbol{1+GK}}\right\|_\infty$

As in Figure 6.6. of the H-infinity controller, the current on the ac side and the dc link voltage are fed to the controller which generates a control signal for the switching function S_d, S_q. Assuming the input ac signal e_d as constant, the error from the reference input is compensated by W_1 and W_2 enhances the system performance.

The user defined parameters of the PSO and ABC algorithm for this optimization procedure are given in Table 6.2. PID and FOPID controller parameters and the weight variables of the loop shaping controller determined by the optimization algorithms so as to minimize the objective function in (6.31) are listed in Table 6.3.

Table 6.2. Parameters of the PSO and ABC algorithm for robust controller tuning.

PSO	
Parameter	**Value**
Swarm size	40
No. of runs	50
c_1,c_2	2.2,2.1
$[w_{max},w_{min}]$	[0.9,0.4]
ABC	
Parameter	**Value**
Colony size, n_c	40
No. of employed or onlooker bees, N	20
No. of runs, Maxiter	10-40
Limit	60
No. of dimensions in the particle, d	4

The minimized values of the objective function and the execution time of the optimization program in MATLAB in terms of CPU time for the comparative analysis of PSO and ABC optimization algorithms have also been given in this table. It is worthy to mention that the ABC optimization algorithm proves to be better than the PSO algorithm in terms of both reduced CPU time and minimum objective function values attained. Thus, ABC tuned controller variables are used in this work for further analysis.

Further analysis of the loop shaping control scheme achieved through optimization based weight selection shows its efficiency in controller design formulation. The singular value plots in Figure 6.7. (a) and 6.7. (b), enhances the graphical interpretation of the loop shaping inequalities as in (23)-(24), when evaluated for the system under consideration. The sigma plot of sensitivity function shows an increasing slope from 1 rad/sec to around

100000 rad/sec which is always lower to the sigma plot of inverse W_1 function as in Figure 6.7.(a). Similarly, Figure 6.7. (b) shows a constant singular value for complementary sensitivity function till 10000 rad/sec which is lower to the sigma plot of inverse W_2 function. Figure 6.7. (c) demonstrates the complementary behaviour of the *S* and *T* functions with their sum being always equal to one as in equation (6.28). For a range of frequencies from 10^2 to around 10^6 rad/sec the sensitivity is observed to be an increasing function whereas, complementary sensitivity is a decreasing function.

The overall analysis of an efficient loop shaping controller design for the interlinking controller can be determined from the frequency plot in Figure 6.7. (d) which clearly demonstrates the trade-off achieved between performance and robustness such that $\sigma(W_1)$ gives the performance bound for disturbance attenuation and $\sigma(W_2)$ gives the robustness bound for good stability margins.

6.3.2 H-infinity loop shaping controller order reduction

The augmented plant for the interlinking converter system consists of nine states formed by the three states each contributed by the open loop converter state space and the weight functions W_1 and W_2. Thus, the H_∞ controller designed for the interlinking converter is also of the same 9^{th} order which can easily be reduced to its lower order equivalent by any of the direct techniques available in MATLAB. In this work, the controller has been reduced to its 4^{th} order equivalent by Schur-based MATLAB function [108-110] such that a reduced order controller depicts similar performances in time and frequency domains as seen in Figure 6.8.

Table 6.3. Optimized parameters for PID, FOPID and H_∞ Loop shaping controllers.

Control		k_P	k_I	k_D	λ	μ	$J(G,K)$	***CPU Time (sec)***	
PID	*PSO*	0.000922	0.000000	0.000279	1	1	7.788548	218.373	
	ABC	0.001355	0.000010	0.000161	1	1	5.716538	48.714	
FOPID	*PSO*	0.000922	0.000000	0.000098	1.06	1	4.903054	151.914	
	ABC	0.009392	0.000000	0.000097	0.90	1	4.225641	58.294	
		a	b	g	ω_{BW}	h			γ
H_∞ Loop Shaping	*PSO*	5.406598	0.044856	136.313435	1589	0.0001	0.493853	319.307	0.494
	ABC	2.527076	0.159634	83.681150	951	0.0001	0.131013	300.991	0.128

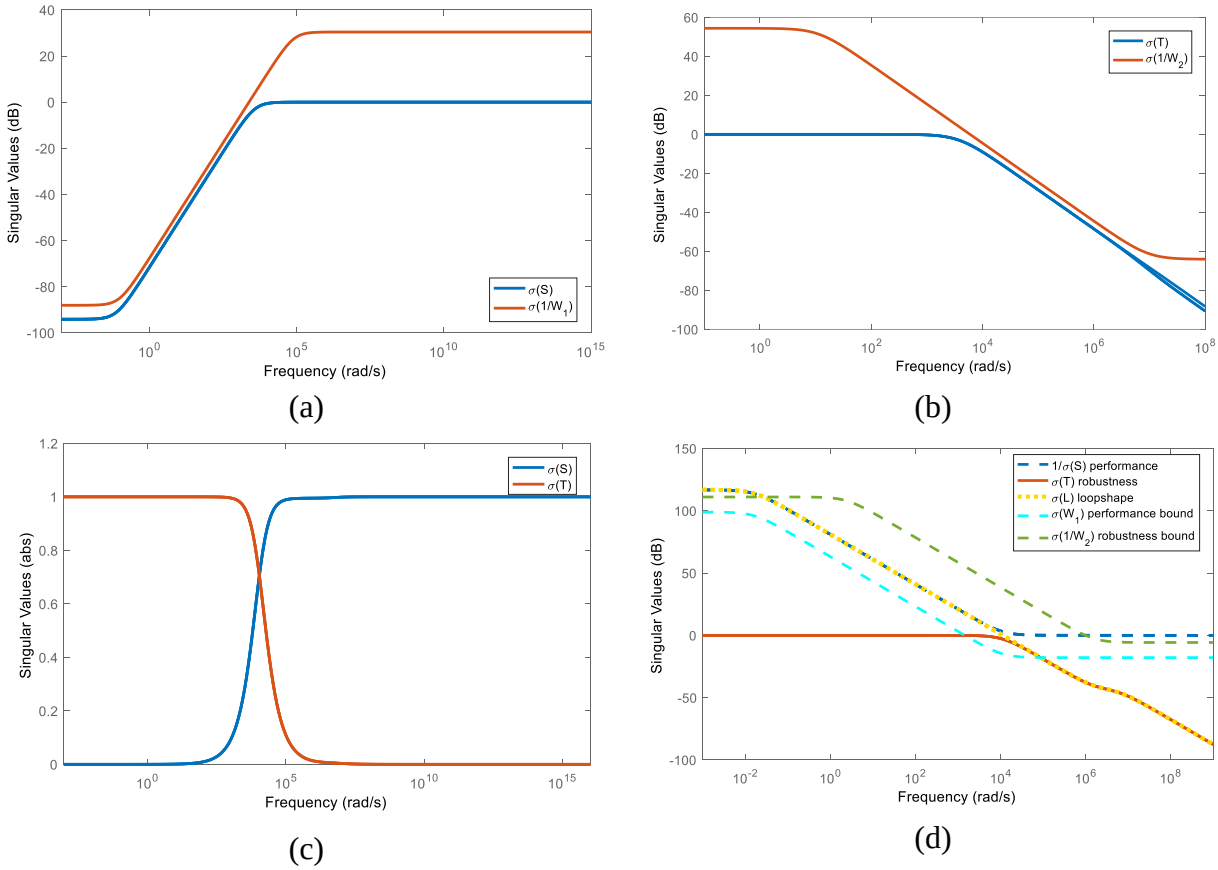

Figure 6.7. *Singular value plots for sensitivity and complementary sensitivity functions along with corresponding weights and loop shaping control.*

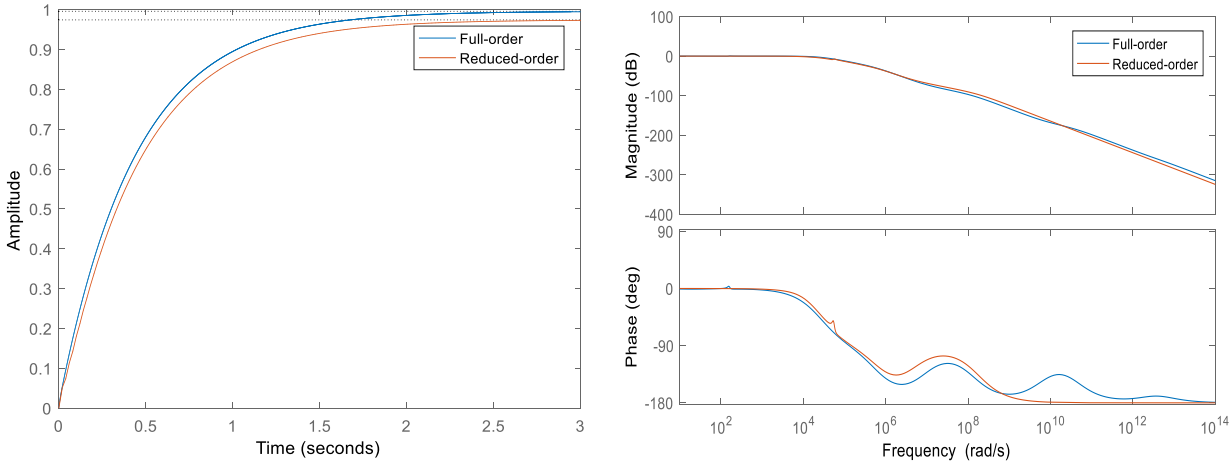

Figure 6.8. *Time and frequency response of closed loop system with full order and reduced order H-infinity controller.*

The efficiency in order reduction is shown in Figure 6.9. (a) with the coincident singular values of reduced order controller K_{red} to the full order controller K over all the operating frequencies.

The constraints in loop shaping controller design remain intact with the controller order reduction as demonstrated in Figure 6.9.(b), where the sensitivity and complementary sensitivity functions with reduced order controller can be seen to follow the ones with full order controller.

6.3.3 Case Study of different controller responses

A case study of the system responses with the three optimisation based controllers; PID, FOPID and H-infinity loop shaping with changes in input, system states and operating conditions are discussed below.

CASE 1:

Closed loop response of d-axis inductor current with a step change in switching.

The closed-loop response of i_d with change in the switching sequence S_d for three of the controllers: PID Controller, FOPID Controller and H_∞ loop shaping controller, designed for interlinking converters is shown in Figure 6.10. The closed loop response of H-infinity controller shows a reduced settling time as compared to the other two controller responses with peak overshoot being the same as that for a PID controller.

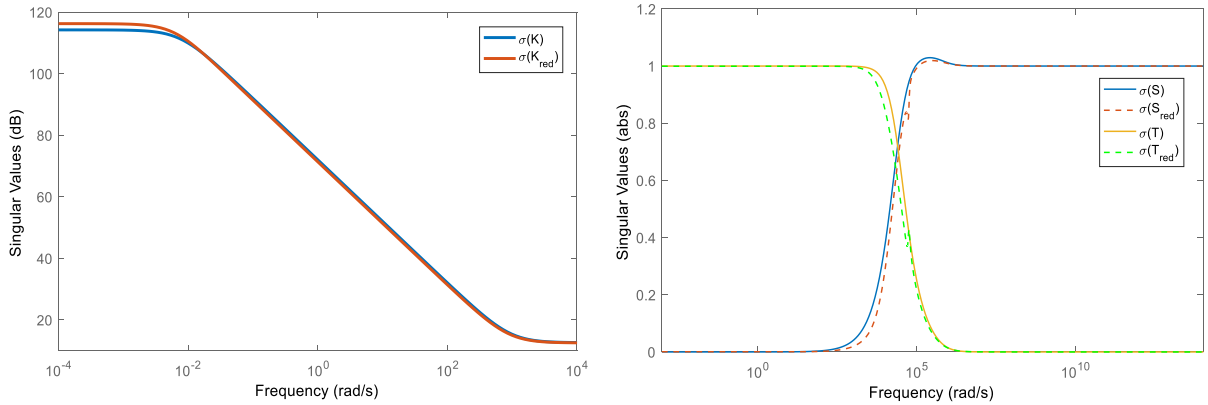

(a) (b)

Figure 6.9. *Singular values of full order and reduced order H_∞ controller and their sensitivity functions for the system under consideration.*

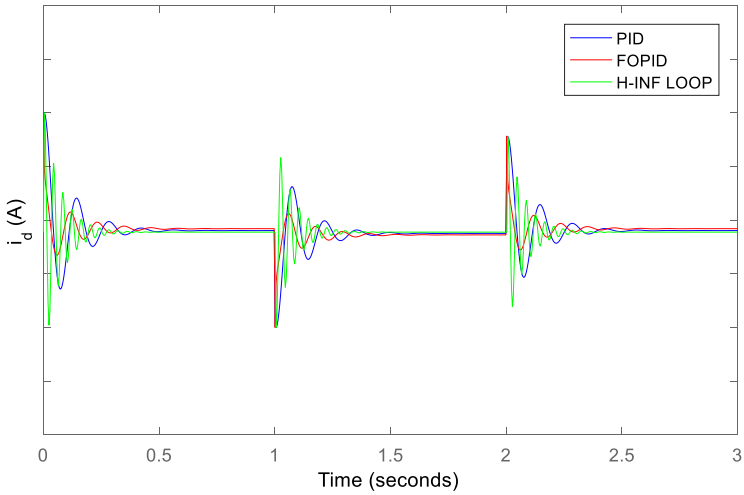

Figure 6.10. *Inductor current (d axis) with step changes in switching.*

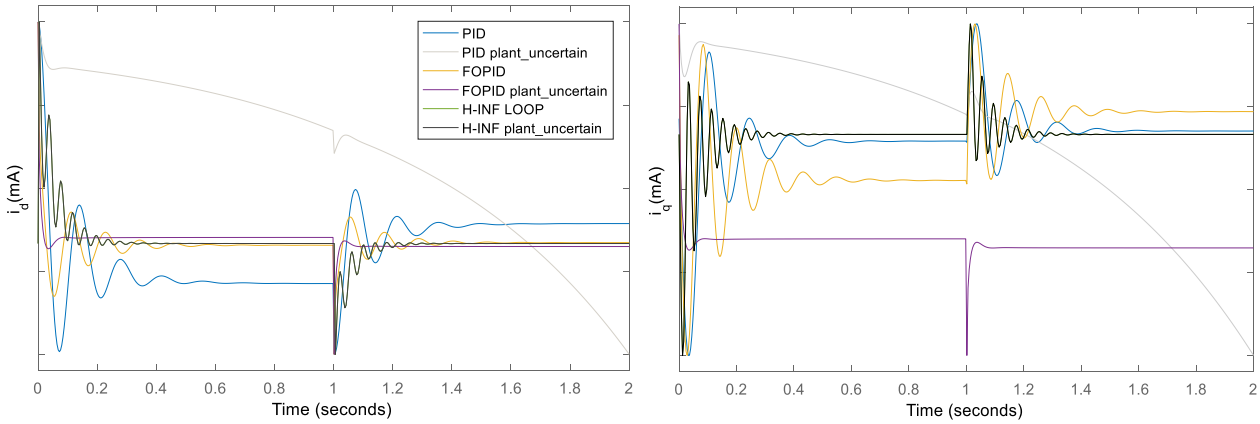

(a) **(b)**

Figure 6.11. *Inductor current (dq) with a change in plant parameter.*

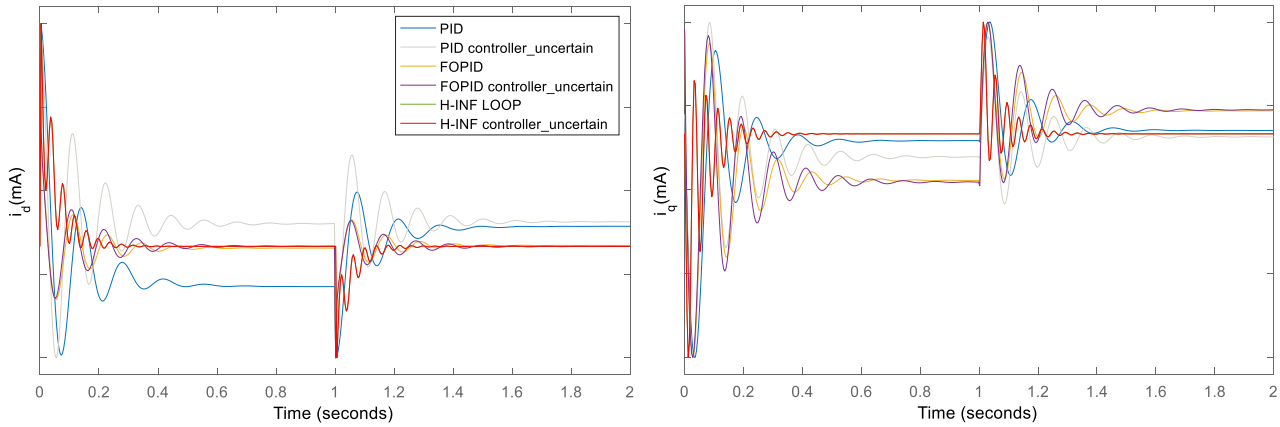

(a) (b)

Figure 6.12. *Inductor current (dq) with a change in the controller parameter.*

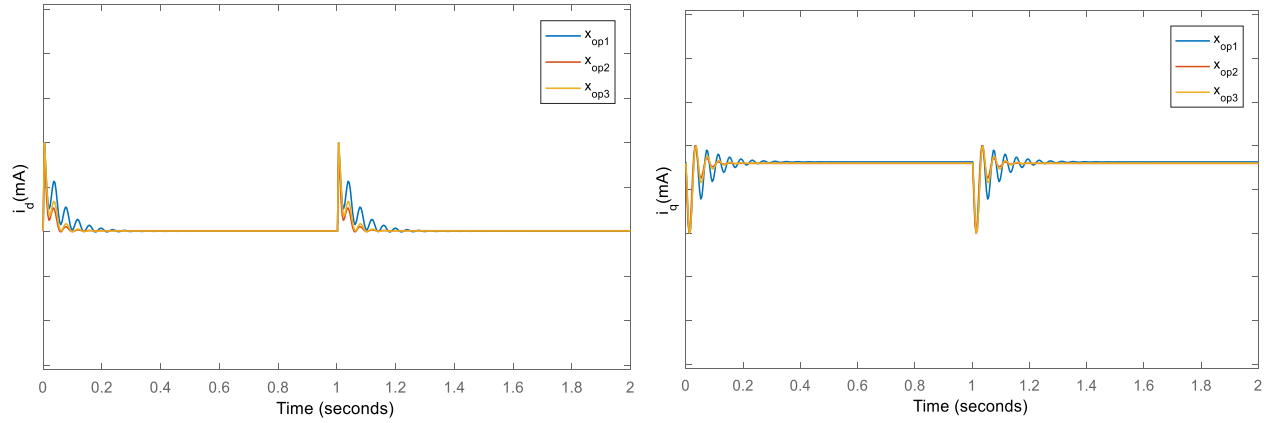

(a) (b)

Figure 6.13*. Inductor current (dq) with a change in plant operating point.*

CASE 2:

Closed-loop responses with a change in plant parameter.

With a fixed change in plant, for e.g., change in resistance on ac side to 10 ohms, the responses for dq-inductor currents shown in Figure 6.11., indicates that the loop shaping controller behaviour remains the same. The responses have been shown with the step disturbance in the input v_d at the starting and after 1 second. The uncertainty causes

the PID controller responses to become unstable whereas the FOPID responses deviate in their steady state values.

CASE 3:

Closed-loop responses with a change in the controller parameter.

With a fixed uncertainty in controller parameters, for e.g., scaling in parameters by 10 times, the responses for dq-inductor currents shown in Figure 6.12., indicates that the loop shaping controller behaviour remains the same. The responses have been shown with the step disturbance in the input v_d at the starting and after 1 second. The uncertainty causes the PID controller responses and the FOPID controller responses to deviate in their steady state values with larger deviation in PID than in FOPID response.

CASE 4:

Change in operating points with loop shaping controller.

The operating point of the plant can change due to many reasons such as, environment changes, component errors, power mismatches etc. Figure 6.13. shows the closed loop responses of dq-inductor currents for loop shaping controller with three different operating points for the interlinking converter system.

The three operating points considered for the plant are;

$$x_{op1} = [75.92071 - 37.99367 - 299.82019];$$

$$x_{op2} = [25.32752 - 12.66924 - 49.35576];$$

$$x_{op3} = [37.98270 - 19.00380 - 111.99919] \quad (6.32)$$

It can be seen from the figure that there are no significant changes in controller responses with different operating points.

6.4 Eigenvalue Analysis

An eigenvalues analysis determines the various system characteristics which help in the study of system dynamics and stability. Two categories of modes can be distinguished based on real and complex eigenvalues namely; non-oscillatory mode and oscillatory mode respectively. The frequency of oscillation for oscillatory modes is obtained from the imaginary part of eigenvalues whereas, the real part of eigenvalues gives the damping effect of that root on the system as in equation (5.3).

The eigenvalues of the open loop IC system and closed loop system with an H-infinity loop shaping controller are presented in Table 6.4. Since all the roots have negative real parts, thus, the necessary condition for small signal stability, i.e., $\sigma_i < 0$, is fulfilled. The table also enlists the various operating modes with their corresponding damping and oscillations. Two modes have been identified in the open loop system whereas, almost 10 modes exist in the closed loop system. In both the open loop and H_∞ based closed loop system, mode 1 is the oscillatory mode contributing to the frequency of oscillation to the system as 25.2113 Hz and 25.7342 Hz respectively.

Apart from the eigenvalues, the closed loop time responses in Figure 6.10.-6.13. and the frequency responses of two transfer functions i_d/v_d and i_q/v_d shown in the Figure 6.14., also demonstrates the stable performance of the overall system. The frequency response of PID and FOPID are similar in behaviour as opposed to the loop shaping controller response. The responses from loop shaping controller exhibits a larger stability margins than the other two controllers. Thus, loop shaping controllers exhibit

more robustness and tend to remain in stable region despite uncertainties in system and operating conditions.

Table 6.4. Eigenvalues of open loop and closed loop system with H-infinity controller.

Index	***Real part ± jImaginary part***	***Oscillatory Mode***	***Non-oscillatory Mode***	***Damped frequency, f_i(Hz)***	***Damping ratio, ξ***
		OPEN LOOP SYSTEM			
1	-20.7983	0	2		1
2,3	-13.9226	158.326	1	25.2113	0.0876
		CLOSED LOOP SYSTEM			
1,2,3	-95.100×10^{-3}	0	2		1
4,5,6	-9.5100×10^{6}	0	3		1
7	-22.055×10^{12}	0	4		1
8	-185.645×10^{9}	0	5		1
9	-614.326×10^{6}	0	6		1
10	-9.814×10^{6}	0	7		1
11	-7.399×10^{6}	0	8		1
12	-7.401×10^{6}	0			1
13,14	-8.605	161.611	1	25.734	0.053
15	-18.603	0	9		1
16	-3.795×10^{3}	0			1
17	-3.781×10^{3}	0	10		1
18	-3.782×10^{3}	0			1

6.5 Summary

Robust controller design for an AC-DC IC state space model with three states, namely, i_d, i_q and v_{dc}based on parameter tuning by optimization algorithms: PSO and ABC, has been presented. PID, FOPID and H-infinity loop shaping controllers have been

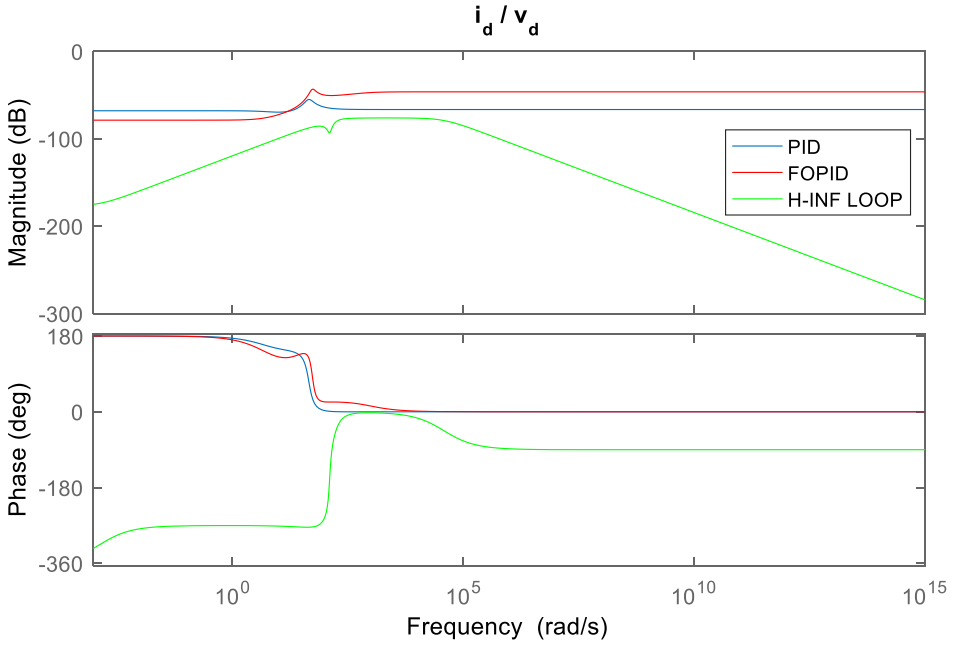

(a)

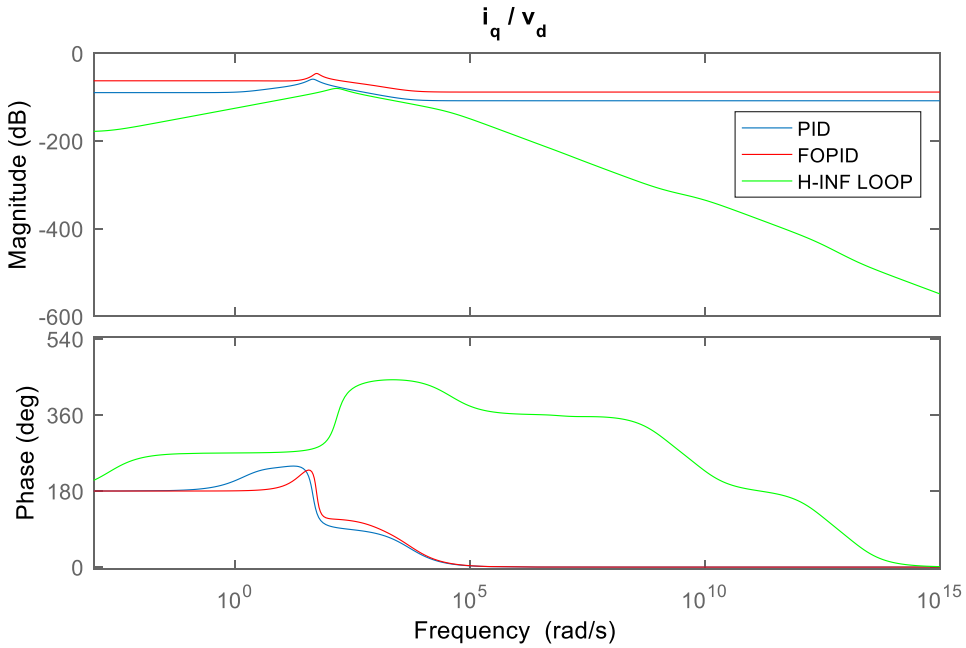

(b)

Figure 6.14. *Bode-plot for PID, FOPID and loop shaping controller based closed-loop transfer functions for inductor currents.*

designed by optimization of their parameters to attain a reduced H_∞-norm of the closed loop system with controller.

The various constraints on loop shaping controller design and weight functions has been discussed to obtain the optimal weights through optimization so as to achieve the desired trade-off between performance and disturbance rejection. The designed controllers achieve the desired objective of proper control of switching pulses for regulation of ac inductor currents and dc link capacitor voltage. Further, reduction in order of the loop shaping controller from 9^{th} to 4^{th} order controller does not alter the controller performance to a large extent. All these simulation results have been evaluated in the MATLAB environment. An eigenvalue analysis and its associated linearized stability concerns have also been taken into consideration.